AIChE WILEY InterScience DISCOVER SOMETHING GREAT

BIOENGINEERING, FOOD, AND NATURAL PRODUCTS

Modeling Gas Displacement Kinetics in Coal with Maxwell-Stefan Diffusion Theory

X. R. Wei, G. X. Wang, P. Massarotto, and V. Rudolph
Division of Chemical Engineering, The University of Queensland, Brisbane, QLD 4072, Australia

S. D. Golding
Division of Earth Sciences, The University of Queensland, Brisbane, QLD 4072, Australia

DOI 10.1002/aic.11314
Published online October 29, 2007 in Wiley InterScience (www.interscience.wiley.com).

The kinetics of binary gas counter-diffusion and Darcy flow in a large coal sample were modeled, and the results compared with data from experimental laboratory investigations. The study aimed for a better understanding of the CO_2-sequestration enhanced coalbed methane (ECBM) recovery process. The transport model used was based on the bidisperse diffusion mechanism and Maxwell-Stefan (MS) diffusion theory. This provides an alternative approach to simulate multicomponent gas diffusion and flow in bulk coals. A series of high-stress core flush tests were performed on a large coal sample sourced from a Bowen Basin coal mine in Queensland, Australia to investigate the kinetics of one gas displacing another. These experimental results were used to derive gas diffusivities, and to examine the predictive capability of the diffusion model. The simulations show good agreements with the displacement experiments, revealing that MS diffusion theory is superior for describing diffusion of mixed gases in coals compared with the constant Fick diffusivity model. The optimized effective micropore and macropore diffusivities are comparable with experimental measurements achieved by other researchers.
 AIChE J, 53: 3241–3252, 2007
Keywords: coalbed methane, CO_2 sequestration, gas displacement, gas diffusion, kinetics, modeling

Introduction

The displacement kinetics of gas mixtures in coals is of great importance for the simulation of ECBM production. However, when dealing with displacement kinetics, problems arise due to incomplete understanding of multicomponent gas diffusion and Darcy flow processes in coals. This difficulty is partly attributed to the complexity of multicomponent gas counterdiffusion and flow occurring during the ECBM process and the effect of the structural heterogeneity of coal.[1,2]

The pore structure of coal is highly heterogeneous and varies with coal type and rank.[2] Currently two classes of pore structure models have been proposed for evaluation of effective diffusion coefficients in coals with multiscale pore space: the Bethe network model based on percolation concepts,[3,4] and the two-phase random pore model.[5] Bhatia[5] compared four different random pore structure models with the experimental data of Nandi and Walker; [6] his analysis suggested that the pore structure model proposed by Ruckenstein[7] is the most appropriate for coals.

Gas diffusion in coals is significantly influenced by coal rank and lithotype, microstructure and secondary mineralization.[8–10] Theoretical and experimental studies propose that gas transport in coal seams can be classified into two types:

Correspondence concerning this article should be addressed to G. X. Wang at g.wang@eng.uq.edu.au.

a two-step transport process, involving viscous flow and diffusion; or a multistep transport process, depending on coal type and rank.[9] The multistep process consists of gas diffusion in micropores (<2 nm); gas diffusion through partly blocked microfractures, which may consist of mesopores (2 nm ~ 50 nm) and macropores (>50 nm); viscous gas flow through open, unmineralized microfractures (0.05 ~ 20 μm wide); and then viscous gas flow through the main fractures/cleats (0.1 ~ 2 mm wide). Our premise is that CBM/ECBM production is largely controlled by this overall multistep transport process.

Fracture permeability is recognized as one of the most important parameters for Darcy flow and CBM production. It is primarily controlled by the prevailing net horizontal maximum stress, defined as the difference between the external stress and internal pore pressure.[11] Both experimental and theoretical research indicates that permeability of coal fractures decreases exponentially with increasing net isotropic stress.[12,13] The effect of matrix shrinkage on cleat porosity and permeability has been studied, and has led to several predictive permeability models,[14–18] partially reviewed by Shi and Durucan.[11] In this work, the permeability model proposed by Shi and Durucan[18] was used in the simulations, for convenience, to account for the stress-dependent porosity and permeability.

For a better understanding of gas diffusion and Darcy flow in coals, we have developed a new model to describe gas diffusion in bulk coals. The model embeds a bimodal pore structure in the coal matrix, based on the approach proposed by Ruckenstein et al.[7] In this model, the micropore diffusivity is considered to be dependent on concentration, and the diffusion behavior of mixed gases can be described by using the MS diffusion formulation. This article presents evidence matching the model outputs related to the diffusion and viscous flow of binary gas displacement against laboratory core flood measurements of a large coal sample under various operating conditions. Three displacement tests were chosen for the verification, where He or CO_2 were injected into the coal sample to displace preadsorbed CO_2 or CH_4. The sensitivities of gas diffusion and flow behavior to several uncertain model parameters were analyzed, resulting in improved model inputs for simulation of the displacement kinetics of binary gases in the coal sample.

Theory

The following assumptions are applied to model the gas diffusion and Darcy flow in the coal matrix:

1. The coal matrix is treated as a cylindrical cell surrounded by main fractures (cleats). It contains monosize spherical particles and the interstitial space represents open microfractures (Figure 1a);

2. These particles are themselves formed from smaller monosize spherical microparticles. The interstitial space between the microparticles represents the meso-/macroporosity (Figure 1b). The microparticles contain homogeneous microporosity;

3. Gas flow through open microfractures is assumed to be viscous flow obeying Darcy's law (a water phase is not included in the model);

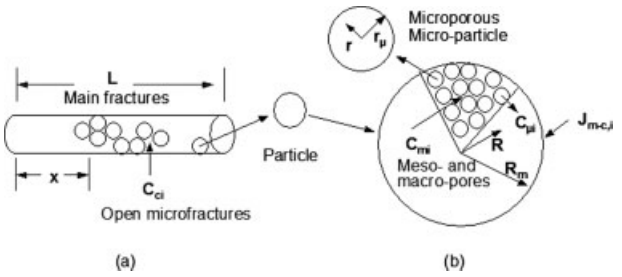

Figure 1. Conceptual model for multi-porosity system: (a) a cylindrical coal matrix, and (b) a particle showing bimodal pore structure.

4. Gas diffusion in the coal matrix is assumed to occur through the bimodal pore structure,[7] which incorporates surface diffusions in micropores along with bulk and Knudsen diffusion in meso-/macropores;

5. The equilibrium between the gas phase and adsorbed phase is instantaneous.

Three levels of mass balance equations can be developed for the three classes of pore size, i.e., open microfractures, meso-/macropores and micropores.

The gas flow in the microfractures can be simplified as 1-dimensional (1-D) Darcy flow, giving

$$\varepsilon_c \frac{\partial(C_{ci})}{\partial t} + \frac{\partial(C_{ci}u_g)}{\partial x} + J_{m-c,i} = 0 (i = 1, 2, \ldots, nc) \quad (1)$$

where C_{ci} is gas concentration in fractures of the gas component i; nc is the number of components; u_g is gas velocity depending on permeability and pressure gradient along the coal matrix cell; ε_c is fracture porosity; and $J_{m\text{-}c,i}$ is mass exchange rate between fractures and particles per unit volume of bulk coal of component i, estimated as

$$J_{m-c,i} = \frac{3\varepsilon_m(1-\varepsilon_c)}{R_m^3}\frac{\partial}{\partial t}\left(\int_0^{R_m} R^2 C_{mi} dR\right) + \frac{9(1-\varepsilon_c)(1-\varepsilon_m)}{R_m^3 r_\mu^3}\frac{\partial}{\partial t}\left[\int_0^{R_m} R^2 \int_0^{r_\mu} r^2 C_{\mu i} dr dR\right] \quad (1a)$$

Multicomponent gas diffusion in meso-/macropores within a particle of radius R_m can be described by

$$\varepsilon_m \frac{\partial(C_{mi})}{\partial t} = -\frac{1}{R^2}\frac{\partial}{\partial R}(R^2 N_{m,i}) - J_{m-\mu,i} (i = 1, 2, \ldots, nc) \quad (2)$$

with initial and boundary conditions

$$t = 0: \; C_{mi} = C_{mi0} \quad (3)$$

$$R = 0: \; \frac{\partial C_{mi}}{\partial R} = 0; \;\; R = R_m: \; C_{mi} = C_{ci} \quad (4)$$

where ε_m is macroporosity; C_{mi} is gas concentration in the particle of the component of i; $J_{m\text{-}\mu,i}$ is mass exchange rate between micropores and meso-/macropores per unit volume of particles of component i, estimated as

$$J_{m-\mu,i} = \frac{3(1-\varepsilon_m)}{r_\mu^3}\frac{\partial}{\partial t}\int_0^{r_\mu} r^2 C_{\mu i} dr \tag{4a}$$

and $N_{m,i}$ is pore diffusion flux in the particle, defined as

$$[N_m] = -[B_m^e]^{-1}\frac{\partial [C_m]}{\partial R} = -[L_m]\frac{\partial [C_m]}{\partial R} \tag{5}$$

where $[L_m]$ is the macropore diffusivity matrix, defined as the inverse of the MS matrix, itself defined as[19]

$$B_m^e(i,j) = \frac{\tau_m}{\varepsilon_m}B_m(i,j) = \frac{\tau_m}{\varepsilon_m}\begin{cases} \dfrac{1}{D_{miM}} + \displaystyle\sum_{\substack{k=1\\k\neq i}}^{nc}\frac{y_k}{D_{mik}} & (i=j; i=1,2,\ldots,nc) \\ -\dfrac{y_i}{D_{mij}} & (i\neq j; i=1,2,\ldots,nc) \end{cases} \tag{6}$$

where τ_m is macropore tortuosity; D_{miM} is Knudsen diffusivity of component i; y_i is molar fraction of component i; and D_{mij} is binary molecular diffusivity between species i and j.

Gas diffusion in micropores within a microparticle of radius r_μ can be described by

$$\varepsilon_\mu \frac{\partial C_{\mu i}}{\partial t} = -\frac{1}{r^2}\frac{\partial}{\partial r}\left(r^2 N_{\mu,i}\right)(i=1,2,\ldots,nc) \tag{7}$$

with initial and boundary conditions

$$t=0: \quad C_{\mu i} = C_{\mu i 0} \quad (r < r_\mu) \tag{8}$$

$$r=0: \ \frac{\partial C_{\mu i}}{\partial r} = 0 \ (i=1,2,\ldots,nc) \tag{9}$$

$$r=r_\mu: \ C_{\mu i} = I_{\mu i}(p,y_i)(i=1,2,\ldots,nc) \tag{10}$$

where $I_{\mu i}(p, y_i)$ is the adsorption equilibrium which can be estimated using IAS-RG/Langmuir approach;[20] ε_μ is the microporosity; $C_{\mu i}$ is gas concentration in the microparticle of the component i; $N_{\mu,i}$ is the surface diffusion flux in the microparticle, which can be approximated using the model proposed by Krishna in 1990,[21] giving

$$[N_\mu] = -[B_\mu^e]^{-1}[\Gamma]\frac{\partial [C_\mu]}{\partial r} = -[L_\mu]\frac{\partial [C_\mu]}{\partial r} \tag{11}$$

where $[\Gamma]$ is a matrix of thermodynamic factors. The matrix of inverted effective MS micropore diffusivities has the elements

$$B_\mu^e(i,j) = \frac{\tau_\mu}{\varepsilon_\mu}B_\mu(i,j) = \frac{\tau_\mu}{\varepsilon_\mu}\begin{cases} \dfrac{1}{D_{iV}} + \displaystyle\sum_{\substack{k=1\\k\neq i}}^{nc}\frac{\theta_k}{D_{ik}} & (i=j; i=1,2,\ldots,nc) \\ -\dfrac{\theta_i}{D_{ij}} & (i\neq j; i=1,2,\ldots,nc) \end{cases} \tag{12}$$

where τ_μ is micropore tortuosity; θ_i is fractional surface coverage; D_{iV} and D_{ij} are MS micropore diffusivity of component i and MS counter-diffusivity between components i and j, respectively.

The values of fracture porosity and permeability may vary during the tests due to coal matrix shrinkage and swelling. To evaluate the variations of stress-dependent permeability and porosity for a multicomponent system under a condition of stressed sorption, a variety of models are available. The Shi-Durucan (SD) model[11,18] was used here for convenience, describing the change in effective horizontal stress, as

$$\sigma - \sigma_0 = \frac{v}{1-v}(p-p_0) + \frac{E}{3(1-v)}\sum_{i=1}^{nc}\alpha_{si}\left(C_{\mu i} - C_{\mu i0}\right) \tag{13}$$

where σ is effective horizontal stress; v is Poisson ratio; E is Young's modulus; α_{si} is matrix shrinkage/swelling coefficient of component i; p is the pore pressure. σ_0, and p_0 are initial effective horizontal stress and pore pressure, obtained from measurements in the rock surrounding the seam, either by over coring,[22] or by hydrofracture.[23] Using the extended Langmuir isotherm, the adsorbed volume for gas component j may be approximated by

$$C_{\mu i} = \frac{V_{Li}p\frac{y_i}{P_{Li}}}{1 + p\sum_{i=1}^{nc}\frac{y_i}{P_{Li}}} \tag{14}$$

where V_{Li} is the Langmuir volume of component i; y_i is the mole fraction of component i in gas phase; P_{Li} is the Langmuir pressure of component i. The fracture porosity varies exponentially with change in the effective horizontal stress[13]

$$\varepsilon_c = \varepsilon_{c0}e^{-c_f(\sigma-\sigma_0)} \tag{15}$$

where ε_{c0} is initial fracture porosity; c_f is cleat-volume compressibility. The fracture permeability can be derived from following relationship[12]

$$\frac{k}{k_0} = \left(\frac{\varepsilon_c}{\varepsilon_{c0}}\right)^3 \tag{16}$$

where k and k_0 are fracture permeability and initial fracture permeability, respectively.

The model discussed in this article describes a coupled system dealing with three different processes: gas sorption equilibrium; gas diffusion and viscous flow; and matrix shrinkage and swelling. Among these processes, gas diffusion and viscous flow is critical, and described via Eqs. 1, 2 and 7. A loose coupling algorithm[24] is adopted in this work for numerical solution of the highly coupled equations. The gas sorption equilibrium and matrix shrinkage/swelling can be solved independently at designated time intervals under the given pressure and concentration. The Eqs. 1, 2 and 7 are numerically coupled through the mass exchange rates $J_{m\text{-}c,i}$ and $J_{m\text{-}\mu,i}$ obtained at previous steps by Eqs. 1a and 4a, respectively. The multicomponent sorption equilibrium was determined using ideal adsorbed solution-real gas (IAS-RG) approach with Langmuir isotherm;[20] and coal matrix shrinkage, and swelling are estimated by Eqs. 13 to 16. The detailed numerical solution procedure can be found in our previous study.[25]

Experiments

In order to investigate the displacement kinetics of binary gas in a coal sample, experiments were conducted in a specially

Table 1. Conditions and Results of Core Flush Tests

Conditions/results	Stage 17	Stage 29	Stage 34
Test	CO_2 displaces CH_4	He displaces CO_2	CO_2 displaces CH_4
Adsorbed pressure ($\times 10^6$ Pa)	0.501	0.50	2.10
Mean pore pressure ($\times 10^6$ Pa)	0.40	0.40	2.00
Displacing time (seconds)	60480.00	62388.00	151092.00
Total displaced gas (NL)	7.49	12.98	17.49
Gas in connection tube (NL)	4.633	4.694	15.825
Free gas in coal sample (NL)	0.181	0.184	0.521
Desorbed gas (STP, NL)	2.591	7.845	1.108
Initial adsorbed gas (STP, NL)	2.67	8.31	7.00
Variation of effective stress ($\times 10^6$ Pa)	3.9 → 4.3	4.1 → 3.2	2.4 → 3.3
Variation of permeability (mD)	3.1 → 2.0	1.7 → 3.6	2.5 → 1.1

designed true triaxial permeameter,[26] which allows the use of large coal samples and can individually control the stresses acting on the sample in three mutually-orthogonal directions. The experiments were core flush tests where CO_2, or He gas was injected into the coal sample to displace preadsorbed CH_4 or CO_2. During the tests gas inlet pressure and flow rate were kept constant, and the composition of downstream gases were continuously analyzed using a Varian 3900 micrgas chromatograph.

The sample tested was cut from a large block originating from an open cut coal mine in the central area of the Bowen basin, Australia. The sample was cut into an 80 × 80 × 80 mm cube, and then stored in polyethylene film until used. Moisture in the sample was about 5%, helium-derived density was 1,285 kg/m^3, and the vitrinite random reflectance (Vro) ranged from 0.97 to 1.06, making it a high volatile bituminous coal. The average face cleat spacing as observed from the top and bottom of the sample was 7 mm; the butt cleat spacing was 8 mm on the lefthand side, and 10 mm on the righthand side.

Total porosity of the coal sample was 0.112, which was measured experimentally using a combination of He pycnometry and Hg porosimetry. Three types of porosities are defined in the model to describe the multiscale porosity system: fracture porosity (ε_c), macroporosity (ε_m) and microporosity (ε_μ). The relative values of these porosities were taken from experimental data on same type of coal. According to previous research[26–28] the total porosity of coal can approximately be divided into microfractures & cleats comprising 11%, meso-and-macropores comprising 36%, and micropores comprising 53%. Although literature data may not exactly match our coal, a sensitivity analysis was carried out to understand how changing porosity allocations affect the outcome. Since the focus of this study is on simulating the displacement kinetics of gases for ECBM recovery, rather than a special investigation of pore structure in a specific coal, the allocated values of subporosities are considered reasonable as input data.

The complete core flood experiments comprised 40 stages, and were performed at room-temperature (298 K). Only three stages are of interest for this study: stressed adsorption of CH_4, then desorption, followed by a stage of CO_2 displacement of remaining CH_4 at low-pressure (400 kPa) (Stage 17). A further test included CO_2 stressed adsorption then desorption, followed by a stage of He displacement of CO_2 at low-pressure (Stage 29). The third test included stressed adsorption of CH_4, followed by a displacement by CO_2 at high 2,000 kPa pressure (Stage 34). Detailed experimental conditions for each of these three stages are shown in Table 1. During each stage, the internal mean pore pressure was kept constant, while the external stress was allowed to increase or decrease from initial conditions to maintain a constant sample volume, as a result of changing effective stress. Variations of permeability with effective stress obtained by experimental measurements are shown in Table 1.

Determination of Kinetic Parameters

Kinetic parameters for meso-/macropores

To use the MS diffusion Eqs. 5 and 6 in modeling gas diffusion through the bulk phase, the binary molecular diffusivities between different species were estimated using the Fuller-Schettler-Giddings correlation,[29] and Knudsen diffusivities of each species were approximated by the analytical formula presented by Jackson.[30] The macropore diffusivity of each species is calculated using the Bosanquet approximation.[30] According to the Bosanquet approximation, the macropore diffusivity of a given species can be estimated from its Knudsen diffusivity and the binary molecular diffusivity

Table 2. Parameter Values Determined by Experiments and Previous Researches

Parameters	Values	Note
Moisture (%)	5.00	These values were determined by experiments.
Helium Density (kg/m^3)	1285.00	
Total porosity (%)	11.22	
Vitrinite random reflectance (Vro)	0.97~1.06	
Face cleat spacing (m)	0.007	
Butt cleat spacing (m)	0.008~0.01	
Cleat porosity (>50 × 10^{-9} m, %)	1.2	These values were estimated according
Mesoporosity (2~50 × 10^{-9} m, %)	4.0	to previous research results for same coal type and
Microporosity (<2 × 10^{-9} m, %)	6.0	rank (high volatile bituminous coal).
Young's modulus (× 10^6 Pa)	0.3 × 10^6	
Poisson's ratio	0.38	

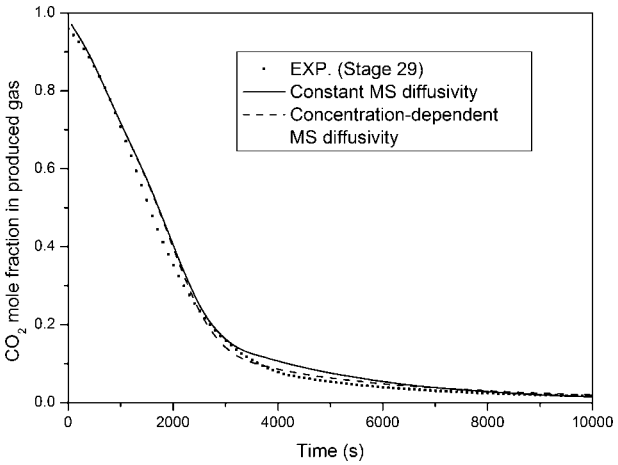

Figure 2. CO_2 mole fraction calculated by the model compared with experimental data.

of the associated binary gas. The values of the kinetic parameters calculated under the conditions of the three stages are shown in Table 2. Several important observations can be drawn from Table 2, summarized as follows:

1. At low to moderate pressures, binary molecular diffusivities vary inversely with pressure, and are independent of pore size;
2. Knudsen diffusivities are independent of pressure and directly proportional to the pore size;
3. Binary diffusivity of gases D_{mij} is normally assumed independent of composition, and they are symmetric, i.e., $D_{m\mathrm{CH4\text{-}CO2}} = D_{m\mathrm{CO2\text{-}CH4}}$;
4. Meso-/macropore diffusivities decrease with increasing pressure, and the diffusivity of CH_4 is larger than that of CO_2.

Kinetic parameters for micropores

The MS micropore diffusivity can be expressed to be dependent on total surface coverage,[19] giving

$$D_{iV} = \frac{1}{z}\lambda^2 v_i(\theta_t) \tag{17}$$

where z is the number of nearest neighbor sites, λ is jump distance, and v_i is jump frequency of component i. When the surface coverage is very low, the jump frequency may remain constant, and the MS micropore diffusivity is independent of surface coverage, thus

$$D_{iV}(0) = \frac{1}{z}\lambda^2 v_i(0) \tag{18}$$

where $v_i(0)$ is the jump frequency at zero surface coverage. As surface concentration increases, the jump frequency decreases with surface coverage due to interaction between adsorbed species.

The heterogeneous macropore surface diffusion model (HMSD) proposed by Do et al.[31] has been used to optimize the surface diffusivity at zero loading $D_{iV}(0)$.[20,31,32] In this work, it is assumed that micropores homogeneously distribute within microparticles, and equilibrium between the gas and adsorbed phases is instantaneous. Therefore, the optimization of MS micropore diffusivity D_{iV} is simplified to fit the experiment with single-component MS diffusion equation

$$D_i = \frac{D_{iV}}{1-\theta_i} \tag{19}$$

where D_i is the apparent surface diffusivity of component i. Eq. 19 is based on a thermodynamic factor assuming Langmuir adsorption.

The test for He displacing CO_2 was modeled to calibrate the MS micropore diffusivity of CO_2. Figure 2 shows the simulation results with an assumption of constant MS micropore diffusivity. It can be seen from the figure that the calculated values of CO_2 mole fraction in the produced gas is larger than the experimental data for most of the test. This may indicate that the predicted micropore diffusivity of CO_2 is larger than the true value. To verify this, we used the following equation to obtain concentration-dependent MS micropore diffusivity

$$D_{iV}(\theta_t) = D_{iV}(0)\left(\sum_{j=1}^{N_0} b_j \theta_t^{j-1}\right) \tag{20}$$

where θ_t is the sum of the fractional surface occupancy of the gas components; b_j ($j = 1, 2, \ldots, N_0$) are coefficients; and $D_{iV}(0)$ is MS micropore diffusivity of component i at zero surface coverage, which can be determined by fitting the calculated results to the experimental data.

The comparisons of results between the conditions of constant MS micropore diffusivity and concentration-dependent micropore diffusivity (Figure 2) show that, although the calculated values under both conditions are equal before about 2,000s of test, a better match with measured gas composition in the produced gas can be obtained after about 3,600s of test, with concentration-dependent micropore diffusivity. The calculated fractional uptakes of CO_2 shown in Figure 3 suggest that the micropore diffusivities calculated using Eq. 20 are less than those obtained with constant diffusivity, which results in a slower diffusion of CO_2. As a result, the matched $D_{iV}(0)$ of CO_2 at 0.4×10^6 Pa is approximately 8×10^{-10} m^2/s. The MS micropore diffusivity of other component is made dimensionless by dividing this by the micropore

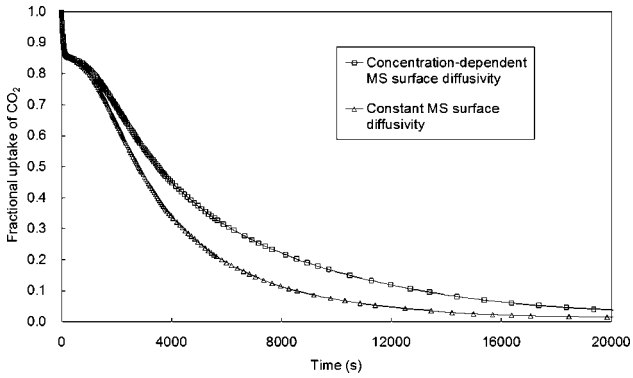

Figure 3. Fractional adsorption of CO_2 calculated by the model.

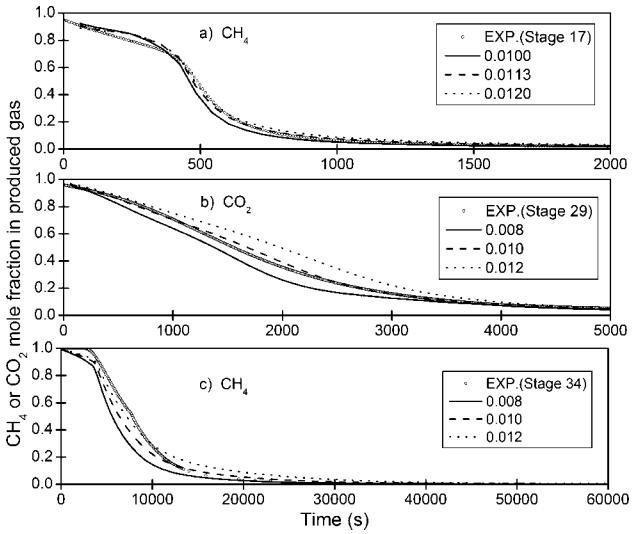

Figure 4. Effects of initial fracture porosity on CH_4 or CO_2 mole fraction in produced gas.

diffusivity of CO_2 at zero surface coverage, giving

$$D^*_{iV}(\theta_t) = D^*_{iV}(0)\left(\sum_{i=1}^{N_0} b_i \theta_t^{i-1}\right) = \frac{D_{iV}(0)}{D_{CO_2V}(0)}\left(\sum_{i=1}^{N_0} b_i \theta_t^{i-1}\right) \tag{21}$$

In this work, the calibration of MS micropore diffusivity of CH_4 is equivalent to calibrating the dimensionless MS micropore diffusivities at zero surface coverage $D^*_{CH_4V}(0)$. Therefore, the unknown parameters in the simulation are dimensionless micropore diffusivities at zero surface coverage $D^*_{iV}(0)$ and $b_i (i = 1, 2, \ldots, N_0)$.

The MS micropore counter-diffusivity can be ignored under the condition of "single file diffusion" following Krishna and Wessingh.[19] However, when counter-diffusion of gases in micropores is important, the MS micropore counter-diffusivity can be estimated using the empirical formulation suggested by Vignes.[19,33]

$$D_{ij}(\theta_t) = \left[D_{iV}\right]^{\theta_i/(\theta_i+\theta_j)}\left[D_{jV}\right]^{\theta_j/(\theta_i+\theta_j)} \tag{22}$$

Sensitivity analysis

The model developed in this study determines the effective macropore and micropore diffusivities by fitting model calculations to experimental data, and, thus, obtains diffusion rates of binary gases. The model results are sensitive to several "uncertain" parameters, such as initial fracture porosity, tortuosities of macropore and micropore, kinetic parameters for micropores. These parameters are evaluated by matching experimental data.

Initial fracture porosity

Generally, the initial fracture porosity of a coal sample can be obtained by experimental measurement. However, the actual value for the coal sample in this study is unavailable. Therefore, we include this as an unknown parameter in the model.

According to previous studies, the initial fracture porosity may account for 11% of total porosity. In this article, it is assumed that adjusting the initial fracture porosity changes the value of initial meso-/macroporosity only, because the value of microporosity is relatively certain. The model results indicated changing the initial fracture porosity has minor effects on gas diffusion rates, but major effects on Darcy flow as shown in Figure. 4. As seen from Figure4a, the calculated results with initial fracture porosity of 0.0113 achieved a good match with experimental data for Stage 17. Similar results have been obtained for Stages 29 and 34 (refer to Figures 4b and c), which indicated that the matched initial fracture porosities for both of these two stages were 0.01 approximately. These values of initial fracture porosity were thought to be reasonable, and used as primary parameters in simulation for the three stages, respectively.

Tortuosity

Tortuosity describes the ease of diffusion and fluid flow through a porous medium. It can be thought of as the ratio of the average pore length L_e, to the length of the porous medium L, along the major flow or diffusion axis. Hence, tortuosity is always greater than 1. Two types of tortuosity are defined as in Eqs. 6 and 12, i.e., macropore tortuosity and micropore tortuosity, to simulate the effective diffusivities in macro- and micropores within coal. It is very difficult to accurately measure the tortuosities. In this work, the tortuosities were estimated by fitting the calculated data of the model to the experimental data.

Figure 5 shows the effects of tortuosities on fractional uptake of CH_4 and CO_2 calculated by the model for Stage 17 of the core flush test. It can be seen from this figure that, when the macropore tortuosity keeps constant, a larger micropore tortuosity would significantly reduce the effective micropore diffusivities of CH_4 and CO_2, and slow CH_4 diffusion out of and CO_2 diffusion into micropores. Similar results are seen for Stages 29 and 34. The effects of tortuosities on gas-flow dynamics for the three stages are shown in Figures 6a to 6c, respectively. It can be seen in Figure 6 that macropore tortuosity has a minor effect on gas diffusion and flow dynamics, while the micropore tortuosity has major effect on gas diffusion and flow rates of CH_4 and CO_2. A larger micropore tortuosity would result in a faster reduction of CH_4 molar fraction

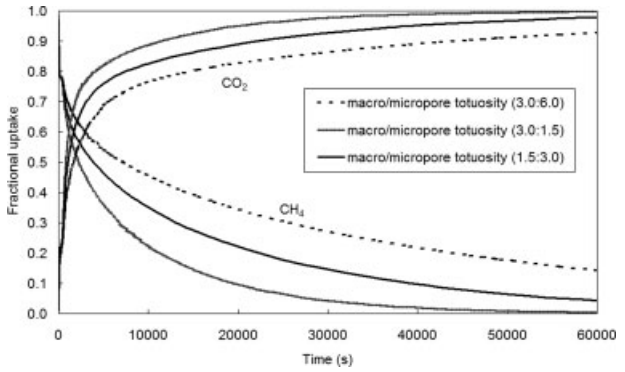

Figure 5. Effects of macropore and micropore tortuosities on fractional uptake for Stage 17.

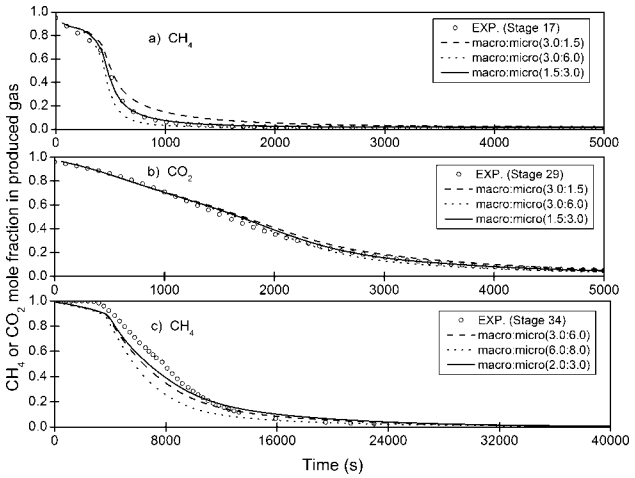

Figure 6. Effects of macropore and micropore tortuosities on gas composition in produced gas.

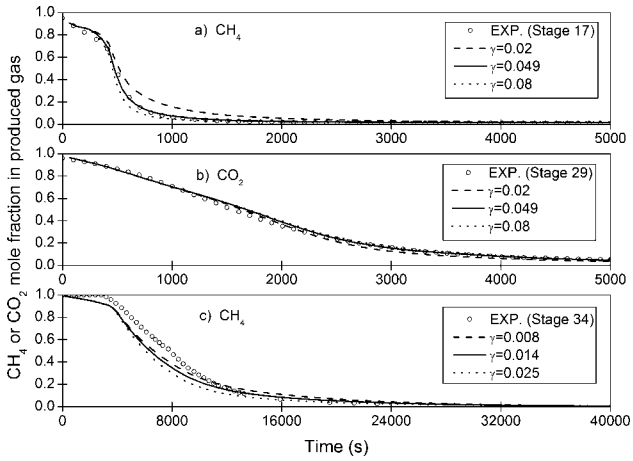

Figure 8. Effects of parameter γ on gas composition in produced gas.

in the initial gas production. This implies that gas diffusion in this coal sample is mainly controlled by the micropore diffusion process. The sensitivity analysis suggests that the macropore tortuosity increases when the system pressure increases. The calibrated macropore and micropore tortuosities for this particular coal are, respectively, 1.5 and 3.0 at 0.4×10^6 Pa, and 2.0 and 3.0 at 2×10^6 Pa.

Ratio of micropore diffusion to macropore diffusion

The ratio of micropore diffusion to macropore diffusion, γ[34] is used to determine effective CO_2 micropore diffusivity. Figures 7 and 8 show the effects of γ on fractional uptake of CO_2, and gas composition in the produced gas.

Higher values of γ give a relatively fast micropore diffusion of CO_2 or CH_4, and, thus, the reduction of CO_2 or CH_4 molar fraction in the produced gas is delayed. Figures 8a to 8c illustrate the simulation results of CO_2 or CH_4 molar fraction for the three stages of the core flush tests, suggesting the matched parameter value of γ is quite different in these three cases. At low-displacement pressures (Stages 17 and 29), the optimized value of γ is 0.049; at a higher displacement pressure, γ is 0.014 (Stage 34).

Ratio of $D_{CH4V}(0)$ to $D_{CO2V}(0)$

The CH_4 micropore diffusivity can be determined by estimating the ratio of micropore diffusivity of CH_4 to that of CO_2, i.e., $D^*_{CH_4V}(0)$. As seen from Figures 9 and 10, if micropore diffusivity of CH_4 is far less than that of CO_2, the diffusion rate of CH_4 would be very slow compared with that of CO_2. A larger value of the ratio will increase the MS diffusivity of CH_4 and MS counter-diffusivity of CH_4-CO_2, and the Fickian micropore diffusivities of CH_4 and CO_2. As a result the CH_4 molar fraction in gas production decreases slowly. Similar results were obtained under the conditions of Stage 34.

Results and Discussion

Model development and parameter reliability

This study investigates the dynamic multicomponent transport process in coal using an overall model consisting of

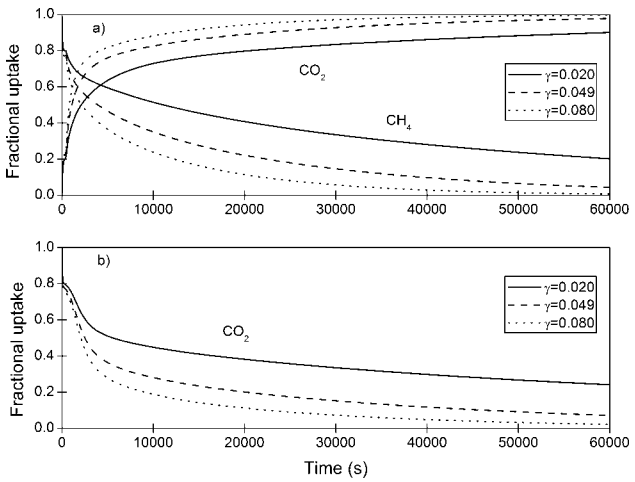

Figure 7. Effects of parameter γ on fractional uptake.

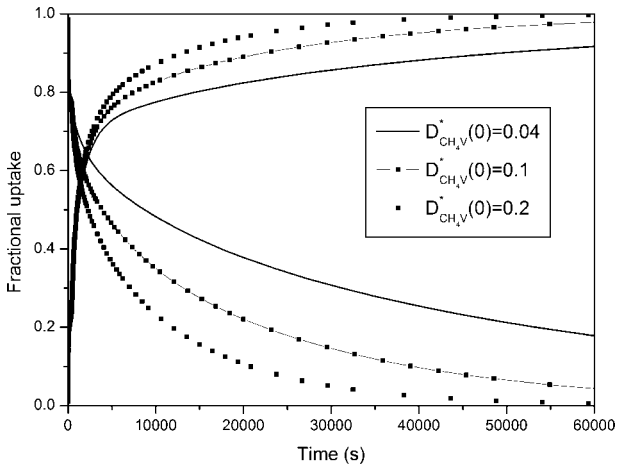

Figure 9. Effects of $D^*_{CH_4V}(0)$ on fractional uptake of CH_4 and CO_2 for Stage 17.

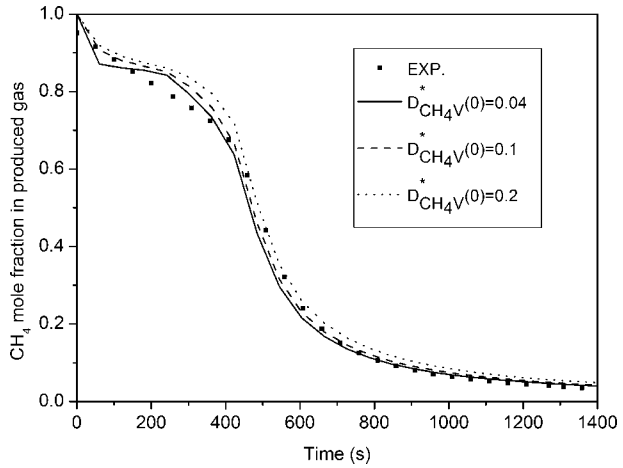

Figure 10. Effects of $D^*_{CH_4V}(0)$ on gas composition in produced gas for Stage 17.

three separate process models in a linear fashion. These process models are used to describe Darcy flow, MS counter-diffusion and coal matrix swelling and shrinkage, respectively. Although there would be several model parameters needed to be estimated for the overall model, our approach allows each process model to use only a few variables at a time in order to achieve reliable results. As well, some parameters, such as matrix shrinkage/swelling coefficients (α_{si} in Eq. 13), and adsorption constants, are directly derived from experiments. The values for the physical properties of coal (initial fracture porosity and tortuosity) can usually be obtained experimentally. This study, however, only focuses on the numerical simulation of the overall transport process in coal by using reasonable values of these properties rather than obtaining the best-fit values from the experimental data; this could be further investigated. The utilized initial fracture porosity and tortuosity were derived from the literature for similar rank coal, and then checked with the gas displacement experiments by sensitivity analyses. The other parameters, $D_{CO_2}V(0)$, γ and $D^*_{CH_4V}(0)$, are used in the MS diffusion model, and are estimated via regression analysis on gas displacement experiments. Following the determinations of these parameters separately, the overall resulting model was then used to predict a theoretical CO_2 displacement of CH_4, thus, no matching was done at this stage.

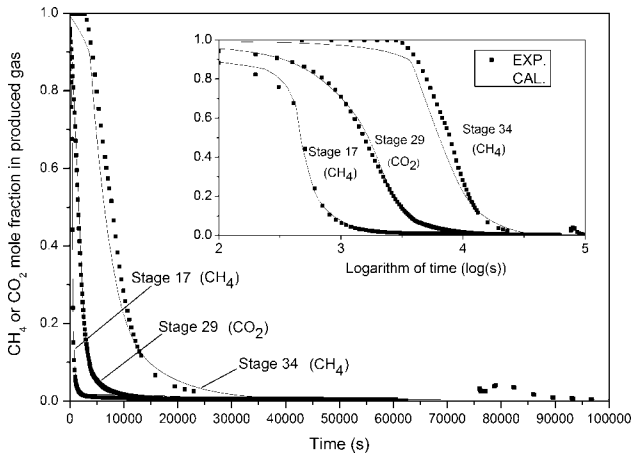

Figure 11. Calculated gas composition in produced gas comparing with experimental data.

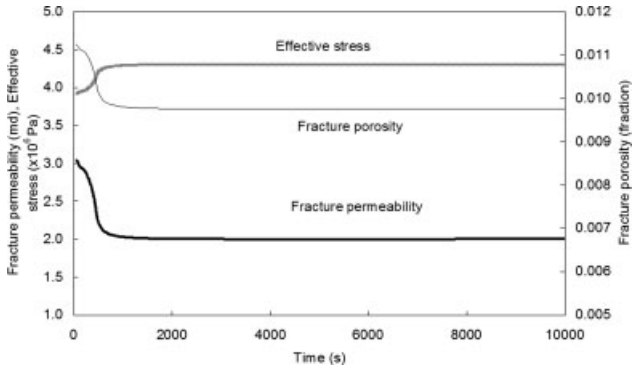

Figure 12. Calculated fracture porosity, permeability and effective stress for Stage 17.

MS diffusion model

The MS diffusion model using fitted model parameters demonstrates the capacity of the model to match the binary gas diffusion process in coal, providing improved predictions of produced gas composition. Figure 11 shows the calculated produced gas composition using the model compared with experimental data for Stages 17, 29 and 34. The modeled results for Stage 34 do not fit the experimental data, as well as for Stages 17 and 29. Unstable operation in early period of Stage 34 was observed based in our lab records, occurring during high-pressure displacement. Therefore, the gas compositions in the produced gas used were obtained by normalizing the initial experimental data. The model results are then basically consistent with adjusted experimental data.

Fracture porosity, permeability and effective stress play important roles in gas diffusion and Darcy flow in coals, and, hence, in the model, the sensitivity to these porosities was checked against the experimental measurements, using the SD permeability model. The calculated results are shown in Figures 12 and 13, which illustrate the dynamic changes of fracture porosity, permeability and effective stress with the

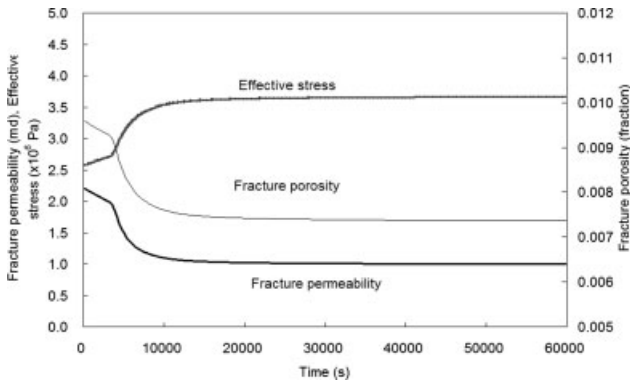

Figure 13. Calculated fracture porosity, permeability and effective stress for Stage 34.

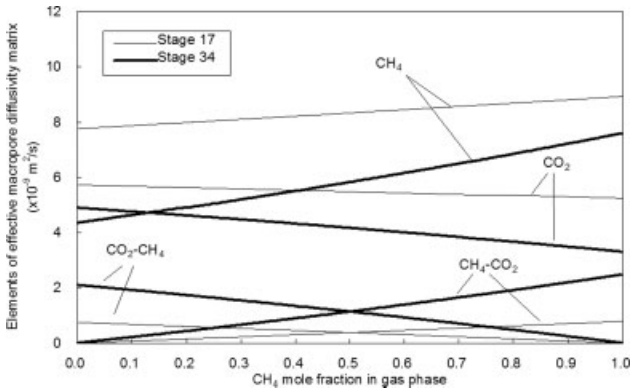

Figure 14. Variations in elements of effective macropore diffusivity matrix [L_m] vs. gas composition in gas phase.

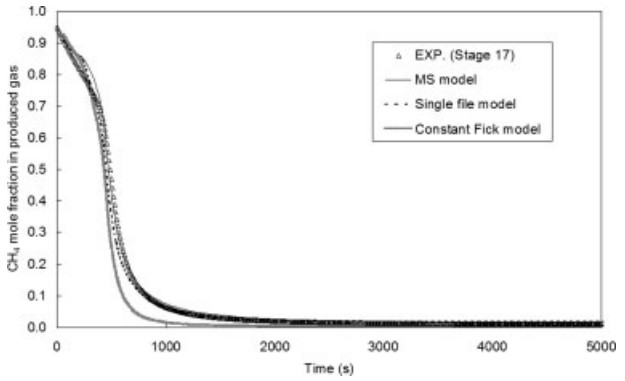

Figure 16. CH_4 mole fraction in gas production calculated by three diffusion models for Stage 17.

time for Stages 17 and 34 of the core flush tests. During these stages, CO_2 was injected into the coal sample, and displaced the adsorbed CH_4 from the coal surface. Since the adsorption capacity of CO_2 is much larger than that of CH_4, the coal matrix swelled due to CO_2 replacement of CH_4; given a constant test volume, the average net stress increased sharply at the early stages, leading to rapid decreases in fracture/cleat permeability and porosity, some 33% and 14%, respectively, for low-pressure Stage 17. The calculated results for high-pressure Stage 34 are a reduction of 55% in permeability and 18% in porosity. The reason for higher losses at higher pressures is that the adsorption capacity of CO_2 increases with pressure, which results in higher swelling of the coal matrix, and larger decreases in fracture porosity and permeability. The swelling and shrinkage of coal matrix induced by adsorption and desorption of gases are unique challenges to deriving accurate and complete gas diffusivities in coals.

Figure 14 shows the effective macropore diffusivities of each component versus gas composition in the gas phase, predicted by the MS diffusion model under the conditions of Stage 34 (similar results were obtained for Stage 17): the effective meso-/macropore diffusivities of CH_4 and CO_2 gradually increase with increasing molar fraction of the corresponding component in the gas phase. However, the variations in effective macropore diffusivities of each component at Stage 34 are larger than those at Stage 17, which suggests that the interaction between CH_4 and CO_2 in counter-diffusion is stronger at higher pressure.

The effective micropore diffusivities of CH_4 and CO_2 under the condition of CO_2 displacing CH_4 at various pore pressures were investigated using the MS diffusion model. Typical results for Stage 17 are illustrated in Figure 15, and show that the effective micropore diffusivities of CH_4 and CO_2 in this binary gas system are functions of the surface mole fraction of CH_4. It can be seen that both CH_4 diffusivity and binary diffusivity of CH_4-CO_2 increase with surface molar fraction of CH_4, while CO_2 diffusivity and binary diffusivity of CO_2-CH_4 decrease, with surface mole fraction of CH_4. These functions are similar to ones obtained by applying the model to Stage 34 shows a consistent trend. However, the predicted values for the micropore diffusivities of gas components at Stage 34 are less than those at Stage 17, which implies that the micropore diffusivities decrease with increasing gas pressure. Moreover, the simulations indicate that CH_4 micropore diffusivity is about 10 times less than

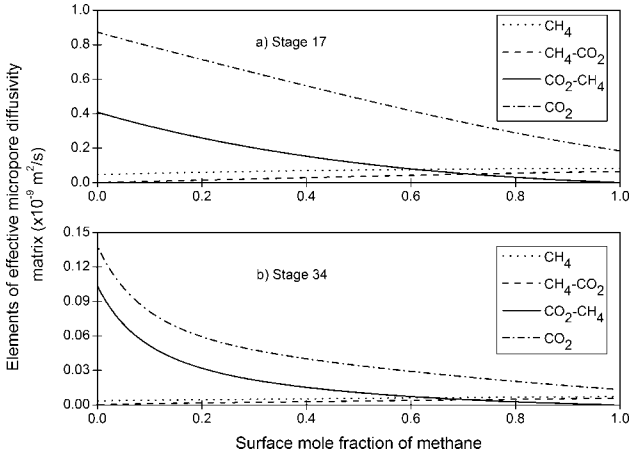

Figure 15. Variations in elements of effective micropore diffusivity matrix [L_μ] vs. surface model fraction.

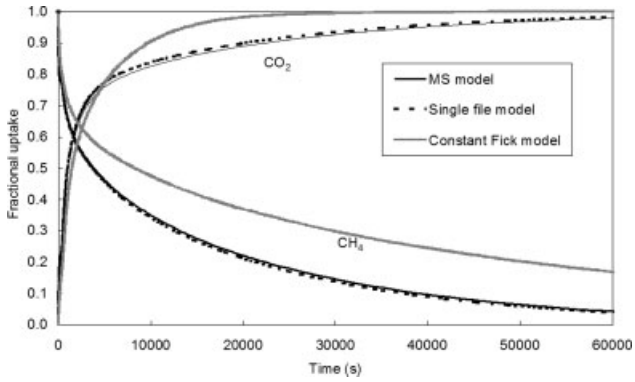

Figure 17. Fractional uptake calculated by three diffusion models for Stage 17.

Table 3. Knudsen, Molecular and Macropore Diffusivities used in Simulation

Stages	Species	Knudsen diffusivity ($\times 10^{-6}$ m^2/s)	Molecular diffusivity ($\times 10^{-6}$ m^2/s)	Macropore diffusivity ($\times 10^{-6}$ m^2/s)
29	He	8.37		5.33
	CO_2	2.57		2.19
	He-CO_2		14.70	
17	CH_4	4.00		2.48
	CO_2	2.57		2.34
	CH_4-CO_2		26.60	
34	CH_4	4.00		2.28
	CO_2	2.57		1.73
	CH_4-CO_2		5.32	

CO_2 micropore diffusivity. The predicted CH_4 effective micropore diffusivities are consistent with experimental measurements.[35]

Comparison with other diffusion models

The MS diffusion formulation for describing gas diffusion and flow dynamics was compared to two other diffusion models, discussed later.

The first comparative model is that proposed by Krishna and Wesselingh,[19] named "single-file diffusion model". It is actually a simplified form of the MS diffusion model. According to this model, Eq. 12 can be simplified as below for comparison with MS diffusion formulation[19,36] giving

$$[B_\mu]^{-1} = \begin{bmatrix} D_{1V} & 0 \\ 0 & D_{2V} \end{bmatrix} \tag{23}$$

The other diffusion model used for comparison is a solid diffusion model with a constant matrix of Fick diffusivities,[36] which is widely used in most of commercial ECBM simulators to describe coal gas diffusion kinetics. The diffusion model is usually expressed as

$$\frac{\partial C_{\mu i}}{\partial t} = D_i \left(\frac{\partial^2 C_{\mu i}}{\partial r^2} + \frac{2}{r} \frac{\partial C_{\mu i}}{\partial r} \right) \tag{24}$$

where D_i is the Fick diffusivity of component i, which is set equal to the Maxwell-Stefan diffusivity at zero coverage. It implies that the unsteady-state diffusion process within the particle is taken into account in solid diffusion model, but on a significantly simplified way, because the model treats Fick diffusivities as constant.

It has been found that the MS diffusion model shows the best agreement with experimental data (Figure 16); this may be attributed to its ability to take gas counter-diffusion in micropores into account. It also confirms that the Vignes relation (see Eq. 22) can be applied in MS diffusion model to provide improved gas displacement kinetics. Figures 16 and 17 also show the comparisons of predicted results by the three-diffusion model. It can be seen that the differences in the simulation results between the MS diffusion model, and MS single-file model are minor, but the constant Fick diffusivity model is generally not very successful in predicting the gas displacement behavior. The methane desorption was underestimated by the constant Fick diffusivity model and carbon dioxide breakthrough in the produced gas was predicted earlier than shown in the experimental data. The dynamics of binary gas-diffusion using either the MS diffusion or the single-file diffusion models seem provide a good match and superior to the constant Fick diffusivity model.

Conclusions

Laboratory core flush experiments on large coal cores, using binary gas counter-diffusion displacements, were incorporated into a complex dynamic multicomponent transport in coal to simulate the CO_2-sequestration enhanced coalbed methane (ECBM) recovery process. The overall transport model was built on three separate process models, in a linear fashion: a Darcy flow model, a Maxwell-Stefan counter-diffusion model, and a coal matrix swelling and shrinkage model. The overall transport model also incorporated a relationship of fracture permeability and porosity with effective stress described by the Shi and Durucan model. Our overall transport model agreed very well with experimental data from the core flush tests. The sensitivity of the model to physical properties and diffusion kinetic parameters of coal has been analyzed, yielding parameters that are partly optimized from matching laboratory results. The use of the MS diffusion model has been validated with the displacement experiments and compared with two other diffusion models. Our modeling results indicate that the MS diffusion theory is superior to a constant Fick diffusivity model for describing binary gas-diffusion dynamics. The predicted micro- and macropore diffusivities show anticipated concentration dependence under various experimental conditions, but also

Table 4. Parameter Values Determined by Fitting Experimental Data

Issues	Parameters	Values	Standard deviation
Kinetic parameters for micropores	D_{CO_2V} (0)	8×10^{-10} m^2/s	0.046
	b_i (i = 1, 2, 3)	1.0, −0.63, 0.15	
Sensitivity analysis	Initial fracture porosity	0.01	
	Macropore and micropore tortuosities	1.5, 3.0 (Stage 17, 29) and 2.0, 3.0 (Stage 34)	
	Parameter γ	0.049 (Stage 17, 29) and 0.014 (Stage 34)	
	$D^*_{CH_4V}$ (0)	0.10	
Simulation results of Stage 17, 29 and 34			0.044, 0.025, 0.25

sensitivity to operating pressure. The optimized values of kinetic parameters may be useful for future modeling of ternary gas mixtures, which occur during flue gas injection ECBM production.

Acknowledgments

This work was supported by the Australian Research Council (ARC), Australian Postgraduate Award (APA) and CSIRO PhD scholarship. Dr. D. Biddle is thanked for his support in providing data from the laboratory displacement experiments.

Notation

$[B_m]$ = matrix of inverted Maxwell-Stefan macropore diffusivities, s/m^2
$[B_\mu]$ = matrix of inverted Maxwell-Stefan micropore diffusivities, s/m^2
b_j = coefficients defined in Eq. 20, dimensionless
C_{ci} = molar concentration of gas component i in open microfractures, mol/m^3
C_{mi} = molar concentration of gas component i in macropores, mol/m^3
C_{mi0} = initial gas molar concentration of component i in macropores, mol/m^3
C_t = total concentration, mol/m^3
$C_{\mu i}$ = molar concentration of component i in micropores, mol/m^3
$C_{\mu i0}$ = initial molar concentration of component i in micropores, mol/m^3
c_f = cleat-volume compressibility, 1/Pa
c_m = matrix shrinkage compressibility due to methane desorption, 1/Pa
c_{ki} = differential swelling coefficients of component i
D_{em0} = initial effective macropore diffusivity, m^2/s
$D_{e\mu 0}$ = initial effective micropore diffusivity, m^2/s
D_{miM} = Knudsen diffusivity of component i, m^2/s
D_{mij} = molecular diffusivity of binary pair i-j, m^2/s
D_{iV} = Maxwell-Stefan micropore diffusivity of component i, m^2/s
D_{ij} = Maxwell-Stefan micropore counter diffusivity between components i and j, m^2/s
E = Young's modulus, Pa
$I_{\mu i}$ = adsorption isotherm
$J_{m\text{-}c,i}$ = mass exchange rate between cleats and bulk coal per unit volume of coals, mol/(m^2 ·s)
$J_{m\text{-}\mu,i}$ = mass exchange rate between micropores and macropores, mol/(m^2 ·s)
k, k_0 = fracture permeability and Initial fracture permeability, respectively, mD
$[L_m]$ = matrix of macropore diffusivities, m^2/s
$[L_\mu]$ = matrix of micropore diffusivity, m^2/s
$[N_m]$ = matrix of molar fluxes in particles, mol/(m^2 ·s)
$[N_\mu]$ = matrix of molar fluxes in microparticles, mol/(m^2 ·s)
nc = number of components in the system
p = pressure, Pa
P_{Li} = Langmuir pressure of component i, Pa
R = particle radial coordinate, m
R_m = radius of particle, m
r = microparticle radial coordinate, m
r_μ = radius of microparticle, m
u_g = velocity of gas-phase, m/s
V_{Lj} = Langmuir volume of component j, mol/m^3
y_i = mole fraction of component i in gas-phase

Greek letters

α_{sj} = matrix shrinkage/swelling coefficient of component j
γ = ratio of diffusion rates in the micropores to that in the macropores
$[\Gamma]$ = matrix of thermodynamic factors
ε_c, ε_{c0} = fracture porosity and initial fracture porosity, respectively
ε_m, ε_μ = Macroporosity and microporosity, respectively
θ_I = fractional surface occupancy of species i
v = Poisson ratio
σ = effective horizontal stress, Pa
τ_m, τ_μ = macropore and micropore tortuosity, respectively

Literature Cited

1. Unsworth JF, Fowler CS, Jones LF. Moisture in coal: 2. Maceral effects on pore structure. *Fuel*. 1989;68:18–26.
2. Laxminarayana C, Crosdale PJ. Role of coal type and rank on methane sorption characteristics of Bowen Basin, Australia. *Intl J of Coal Geology*. 1999;40:309–325.
3. Reyes S, Jensen KF. Percolation concepts in modeling of gas-solid reactions-1. Application to char gasification in the kinetic regime. *Chem Eng Sci*. 1986;41:333–343.
4. Reyes S, Jensen KF. Percolation concepts in modeling of gas-solid reaxtions-2 Application to char gasification in the diffusion regime. *Chem Eng Sci*. 1986;41:345–354.
5. Bhatia SK. Modeling the pore structure of coal. *AIChE J*. 1987;33:1707–1718.
6. Nandi SP, Walker PL. Activated diffusion of methane in coal. *Fuel*. 1970;49:309–323.
7. Ruckenstein E, Vaidyanathan AS, Youngquist GR. Sorption by solid with bidisperse pore structures. *Chem Eng Sci*. 1971;26:1305–1318.
8. Gamson PD, Beamish BB, Johnson DP. Coal microstructure and micropermeability and their effects on natural gas recovery. *Fuel*. 1993;72:87–99.
9. Gamson PD, Beamish BB, Johnson DP. Coal microstructure and secondary mineralization: their effect on methane recovery. In: Gayer R, Harris I. *Coalbed methane and coal geology*. London, United Kingdom: Geological Society of London; 1996:165–179.
10. Crosdale PJ, Beamish BB, Valix M. Coalbed methane sorption related to coal composition. *Intl J of Coal Geology*. 1998;35:147–158.
11. Shi JQ, Durucan S. Drawdown induced changes in permeability of coalbeds: A new interpretation of the reservoir response to primary recovery. *Transport in Porous Media*. 2004;56:1–16.
12. McKee CR, Bumb AC, Koenig RA. Stress-dependent permeability and porosity of coal. In *Coabed Methane Symposium*. 1987. Tuscaloosa, Alabama:183–193.
13. Seidle JP, Jeansonne MW, Erickson DJ. Application of matchstick geometry to stress dependent permeability in coals. In: SPE Rocky Mountain Regional Meeting. 1992. Casper, Wyoming:433–445.
14. Gray I. Reservoir engineering in coal seams: part 1 - the physical process of gas storage and movement in coal seams. *SPE Reservoir Eng*. 1987;2:28–34.
15. Seidle JP, Huitt LG. Experimental measurement of coal matrix shrinkage due to gas desorption and Implications for cleat permeability increases. In 1995 SPE International Meeting on Petroleum Engineering. 1995. Beijing, China:575.
16. Palmer I, Mansoori J. How permeability depends on stress and pore pressure in coalbeds: A new model. In SPE Annual Technical Conference and Exhibition. 1996. Denver, Colorado, U.S.A.:557–564.
17. Pekot LJ, Reeves SR. *Modeling coal matrix shrinkage and differential swelling with CO_2 injection for enhanced coalbed methane recovery and carbon sequestration application*. 2002. Advanced Resources International: Houston, Texas.
18. Shi JQ, Durucan S. A model for changes in coalbed permeability during primary and enhanced methane recovery. *SPE Reservoir Eval and Eng*. 2005;8:291–299.
19. Krishna R, Wesselingh JA. The Maxwell-Stefan approach to mass transfer. *Chem Eng Sci*. 1997;52:861–911.
20. Do DD. *Adsorption analysis: equilibria and kinetics*. London: Imperial College Press; 1998.
21. Krishna R. Multicomponent surface diffusion of adsorbed species. A description based on the generalized Maxwell-Stefan equations. *Chem Eng Sci*. 1990;45:1779–1791.
22. Leeman ER. The determination of the complete state of stress in rock in a single borehole -Laboratory and underground measurements. *Intl J of Rock Mechanics and Mining Sciences*. 1968;5:31–56.
23. Enever JR, Wooltorton BA. Demonstration of hydraulic fracturing stress measurement techniques. In: Lecture Series 59. CSIRO Australia, Division of Geomechanics, Syndal; 1984:1–57.
24. Minkoff SE, Stone CM, Bryant S, Peszynska M, Wheeler MF. Coupled fluid flow and geomechanical deformation modeling. *J of Petroleum Sci and Eng*. 2003;38:37–56.
25. Wei XR, Wang GX, Massarotto P, Golding SD, Rudolph V. Numerical simulation of multicomponent gas diffusion and flow in coals for CO_2 enhanced coalbed methane recovery. *Chem Eng Sci*. 2007;62:4193–4203.

26. Massarotto P. *4-D coal permeability under true triaxial stresses and constant volume conditions*. In: Division of Chemical Engineering, University of Queensland. Brisbane. 2002. PhD Thesis.
27. Gan H, Nandi SP, Walker PL. Nature of the porosity in American coals. *Fuel*. 1972;51:272–277.
28. Levine JR. Coalification: the evolution of coal as source rock and reservoir rock for oil and gas. In AAPG International Conference and Exhibition. 1993. Tulsa, Oklahoma, U.S.A.: the American Association of Petroleum Geologists:39–77.
29. Reid RC, Prausnitz JM, Poling BE. *The properties of gases and liquids*. 3rd ed. New York: McGraw Hill; 1987.
30. Jackson R. *Transport in porous catalysts*. Netherlands: Amsterdam; 1977.
31. Do DD, Hu X. An energy distributed model for adsorption kinetics in large heterogeneous microporous particle. *Chem Eng Sci*. 1993;48:2119.
32. Ding LP, Bhatia SK, Liu F. Kinetics of adsorption on activated carbon: application of heterogeneous vacancy solution theory. *Chem Eng Sci*. 2002;57:3909–3928.
33. Vignes A. Diffusion in binary solutions. *Ind and Eng Chem Fund*. 1966;5:189–199.
34. Liu F, Bhatia SK. Computationally efficient solution techniques for adsorption problems involving steep gradients in bidisperse particles. *Comp and Chem Eng*. 1999;23:933–943.
35. Olague NE, Smith DM. Diffusion of gases in American coals. *Fuel*. 1988;68:1381–1387.
36. Van den Broeke LJP, Krishna R. Experimental verification of the Maxwell-Stefan theory for micropore diffusion. *Chem Eng Sci*. 1995;50:2507–2522.

Manuscript received Dec. 27, 2006, and revision received Aug. 2, 2007.